Electronic Journal of Structural Engineering

Original Article

Cite this: DOI:10.56748/ejse.25791

Received Date: 25 March 2025
Accepted Date: 12 June 2025

1443-9255
https://ejsei.com/ejse

Evaluation of the Rheological Properties of SCC Using Hybrid Random Forest Methods

Junsong Wang [a *]
[a] Wuhan Technical University; Wuhan, Hubei, 430000, China
*Corresponding author: 13871588807@163.com

Abstract

The literature indicates that limited research has focused on predicting both the fresh and hardened properties of self-compacting concrete (SCC). Therefore, this study employs an optimized Random Forest (RF) approach to develop predictive models for both the fresh and hardened properties of SCC. The RF method's determinative variables are optimized by artificial hummingbird optimization (AHA) and grey wolf optimization (GWO) methods. The L-box test, V-funnel test, slump flow, and compressive strength (CS) in the toughened stage are taken into account attributes of SCC in the new stage. Outcomes show strong promise in both training and testing, as well as approximation. It denotes good precision in the training and approximation processes since the relationship among the measured and anticipated SCC qualities from hybrid schemes is satisfactory. Outcomes from AHA-RF outperformed those from GWO-RF and the literature. Generally, the AHA-developed RF scheme serves better than others, demonstrating the AHA tactic's capacity to choose the best variables for the under-consideration technique.

Keywords

Self-compacting concrete, Fly ash, Rheological properties, CS, Random forests

1. Introduction

In 1988, in Japan, SCC was first expanded. These days, SCC is a very efficient concrete blend worldwide (Wang et al., 2022). A kind of concrete known as SCC can load and flow the formatting without the need of external force. As well, it can strengthen by its weight of its own (Garcia-Troncoso et al., 2021). The design combination first concentrated on the two initial requirements, namely the urgency of a high-performing water-decreasing mixture and the need of the great value of superior particle. It requires very little human effort, which is a bonus compared to other types of ordinary concrete. Additionally, it raises result level and lowers noise problems. The SCC technology area is the subject of various research studies, many of which propose tighter increments and continuity. In addition to all these advantages, SCC also has certain drawbacks. The cost of SCC result may be 2-3 times more than that of regular concrete. Therefore, a variety of mixes may be utilized to reduce costs (Esmaeili Falak et al., 2020). These ingredients are utilized in acts as a good substitute for Portland cement (Acharya & Patro, 2015; Beycioğlu & Aruntaş, 2014; Jalal et al., 2015; Sfikas et al., 2014; Sukumar et al., 2008; Yoo et al., 2015). Three different requirements, such as filling capacity, passage capacity, and separation resistance, must be met to prolong SCC. Subsequently certain test trials must be conducted to satisfy these demands. The affordability and cost-effectiveness of SCC are often questioned.

Today, reports of effective artificial neural network usage in several disciplines have been adopted from empirical findings. The concrete industry has greatly increased this use to anticipate diverse concrete qualities. To anticipate the CS of concrete containing silica fume, Oxcan et al. (Özcan et al., 2009) conducted a comparison study examining two approaches, utilizing ANN and fuzzy logic. Many academics recommended suitable examples for comparable applications that were motivated by the Adaptive Neuro-Fuzzy Inference System (ANFIS) to calculate the CS (Douma et al., 2017; Kostić & Vasović, 2015; Shadi & Nazari, 2019; Subaşı et al., 2013). Newly, Sonebi et al. (Sonebi et al., 2016) investigated the novel features of SCC using SVR procedure. Positive and motivating, the output shows finer filling and passing abilities. Various scholars performed similar research work to predict the CS of concrete deploying SVR (Naseri et al., 2017; H. Y. Yang & Dong, 2013; Yazdi et al., 2013). Liu (J. Liu et al., 2016) addressed the idea of specifying autogenous shrinkage of concrete admixtures using an SVM sample. In turn, Yang (S. Yang et al., 2014) investigated corroded reinforced concrete via empirical study. For forecasting the rheological properties of SCC, various schemes have also been established in other articles, including the ANN technique (Douma et al., 2017), M5' and MARS based prediction schemes (Kaveh et al., 2018), and support vector regression (Saha et al., 2020).

It is applicable to address this item in light of the purpose of this investigation's use of the radial basis function neural network (RBFNN) and recently established enhancement technique s (Aljarah et al., 2018; Rashedi et al., 2021). By combining hybrid biogeography-based optimization (BBO) and fuzzy RBFNN, the CS of SCC incorporating FA was anticipated. The outcomes clearly demonstrated that the hybrid model's efficiency in predicting the CS of SCC with FA is satisfactory (Golafshani & Pazouki, 2018). Different research employed a hybrid RBFNN and firefly optimization algorithm (FOA) model to estimate the CS of SCC incorporating Class F FA. The findings show that, in comparison to the empirical findings, the CS anticipated by the suggested schemes performs as expected (Pazouki et al., 2021).

However, almost all of the research on concrete was restricted just to anticipate the toughened concrete characteristics. According to the released publications, only a small amount of research has focused on applying the optimized random forests (RF) approach to anticipate either fresh or hardened characteristics of SCC (Saha et al., 2024; Taffese & Nunes, n.d.). To anticipate fresh and hardened characteristics of SCC using the RF technique, schemes are thus being developed. The Artificial Hummingbird Algorithm (AHA) and Grey Wolf Optimization (GWO) algorithms were used in this work to find the critical variables of the RF technique, which may be improved utilizing optimization methods. To create the GWO-RF and AHA-RF schemes, empirical data records from released publications were acquired.

Several recent studies in civil engineering have explored the use of AHA and GWO for predicting various material properties and optimizing engineering processes (Bi & Yi, 2024). For instance, the GWO has been effectively employed in predicting the compressive strength, flexural strength, and durability indices of concrete, including high-performance and fiber-reinforced types (Dehghanbanadaki et al., 2021; Guangyao et al., 2024; Kalemci et al., 2020; Shariati et al., 2020; Tunca, 2024). GWO has also been integrated with machine learning models such as SVR and ANN to optimize hyperparameters and improve prediction accuracy in applications like chloride diffusion estimation and strength forecasting of blended cements (Bardhan & Asteris, 2023). In parallel, the AHA, although relatively new, has started gaining attention in geotechnical and structural engineering domains (falak & Benmaran, 2024; D. Liu, 2025; Yunpeng et al., 2024). These studies confirm the growing relevance and versatility of AHA and GWO in civil engineering applications, especially when dealing with complex, nonlinear datasets.

The AHA and GWO offer notable advantages over traditional optimization methods, particularly in complex and data-limited engineering problems. AHA excels due to its dynamic foraging strategies, guidance, territorial, and migration, which enhance its exploration-exploitation balance and prevent premature convergence. Its memory-based search mechanism also supports more robust global optimization. GWO, on the other hand, benefits from its simple yet effective leadership hierarchy and hunting behavior, which allows for efficient local refinement and faster convergence with minimal parameter tuning. Compared to other algorithms, both AHA and GWO demonstrate superior adaptability, stability, and performance in high-dimensional, nonlinear problems often encountered in material modeling and machine learning tasks within civil engineering. Their ability to consistently find high-

quality solutions makes them particularly suitable for optimizing predictive models when data is sparse or noisy.

2. Materials and Methods

2.1 Data Description

This investigation aimed to create networks for estimating the parameters connected to SCC's fresh and hardened properties. The majority of the available research has been constrained to evaluate only one actual result attribute utilizing a variety of inputs. Therefore, four outputs of SCC named D flow, L-box, V-funnel, and CS are included. To do this, 114 SCC samples from released publications were collected to create a database (Aggarwal & Aggarwal, 2011; Bingöl & Tohumcu, 2013; Dhiyaneshwaran et al., 2013; Gettu et al., 2002; Güneyisi et al., 2010; Krishnapal et al., 2013; Mahalingam & Nagamani, 2011; Muthupriya et al., 2012; Nepomuceno et al., 2014; Patel, 2004; Şahmaran et al., 2009; Siddique et al., 2012; Uysal & Yilmaz, 2011). Binder (B), fly ash (FA), water to binder ratio (W/B), fine aggregate (FAG), coarse aggregate (CAG), and superplasticizer (SP) are among the concrete elements that are included in the input parameters. The database for this investigation was split into 30% of testing data and 70% of training data (Debnath & Dey, 2018). Table 1 and Fig. 1 provide the database's statistical variables and their histogram plots, respectively.

The association between the two variables is described using the Pearson correlation coefficient (PCC). The outcomes of the relationships are displayed in Fig. 2 (a-d), for DF, LB, VF, and CS, respectively. PCC values that are abnormally high or low make it challenging to assess how explanatory factors have affected the outcome and may indicate that the schemes used are inadequate. The aforementioned factors may account for a considerable portion of the PCCs that are below 0.48, which indicates that they are unlikely sources of multicollinearity problems (Farrar & Glauber, 1967). The highest correlation value is between B and SP at 0.75. The bottom boxes in each figure are related to output variables and inputs. Considering the input variables and outputs related to correlation values, it can be seen that only VF has rough relationship with SP at 0.56.

Table 1. Statistical parameters of variables

Phase	Index	Inputs						Output variable			
		B	FA	W/B	FAG	CAG	SP	DF	LB	VF	CS
Train	$Min.$	370	0.0	0.26	656	590	0.74	510	0.6	2	23
	$Max.$	733	60	0.45	1010	935	21.84	810	1.0	19.2	86.8
	$St.D.$	73.4506	15.74	0.061	92.54	120.486	4.703	53.321	0.084	4.047	17.408
	$Var.$	5394.99	247.67	0.004	8563.65	14517.02	22.12	2843.14	0.007	16.378	303.07
	$Range$	363	60	0.19	354	345	21.1	300	0.4	17.2	63.8
	$Skew.$	0.0869	-0.288	-0.406	-0.272	-0.0644	0.677	-0.0457	-0.52	0.493	0.4955
	$Kurt.$	0.4472	-0.575	-1.059	-1.1257	-1.5461	0.494	0.3045	0.1314	-0.289	-0.908
Test	$Min.$	400	0.0	0.27	686	590	0.86	480	0.6	2.5	17
	$Max.$	628	60	0.45	1038	926	19.53	770	1	14.5	82.9
	$St.D.$	64.463	17.941	0.057	77.842	121.657	4.518	60.735	0.109	3.243	17.251
	$Var.$	4155.556	321.89	0.0033	6059.42	14800.36	20.411	3688.79	0.0120	10.5166	297.59
	$Range$	228	60	0.18	352	336	18.67	290	0.4	12	65.9
	$Skew.$	-0.5276	0.3895	-0.626	-0.219	0.2066	0.496	-0.1246	-0.799	0.1133	0.454
	$Kurt.$	-0.5108	-0.555	-1.055	-0.0220	-1.5411	0.2141	0.8255	0.1453	-1.1721	-0.526

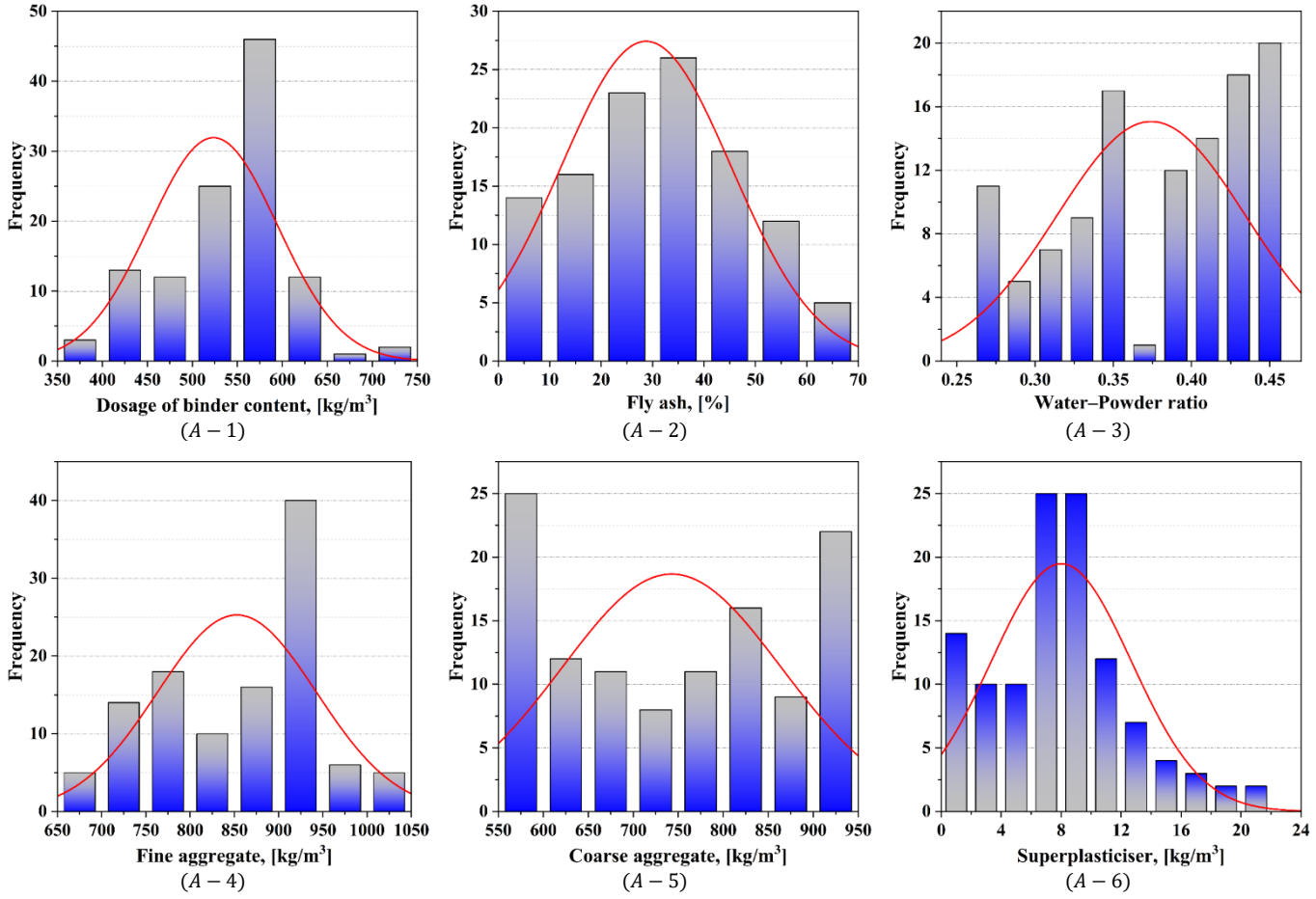

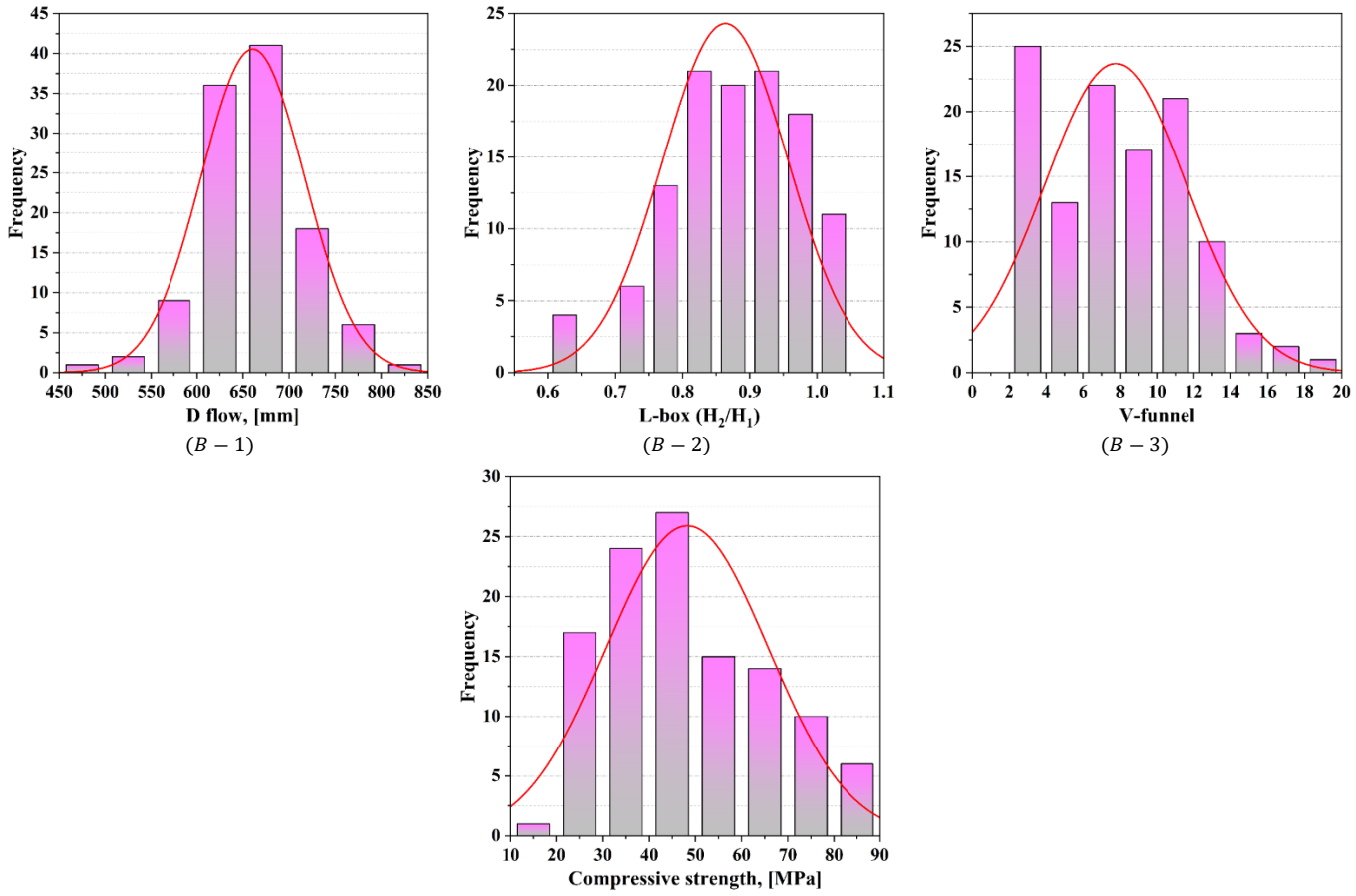

Fig. 1 The histogram plots of the input and output variables

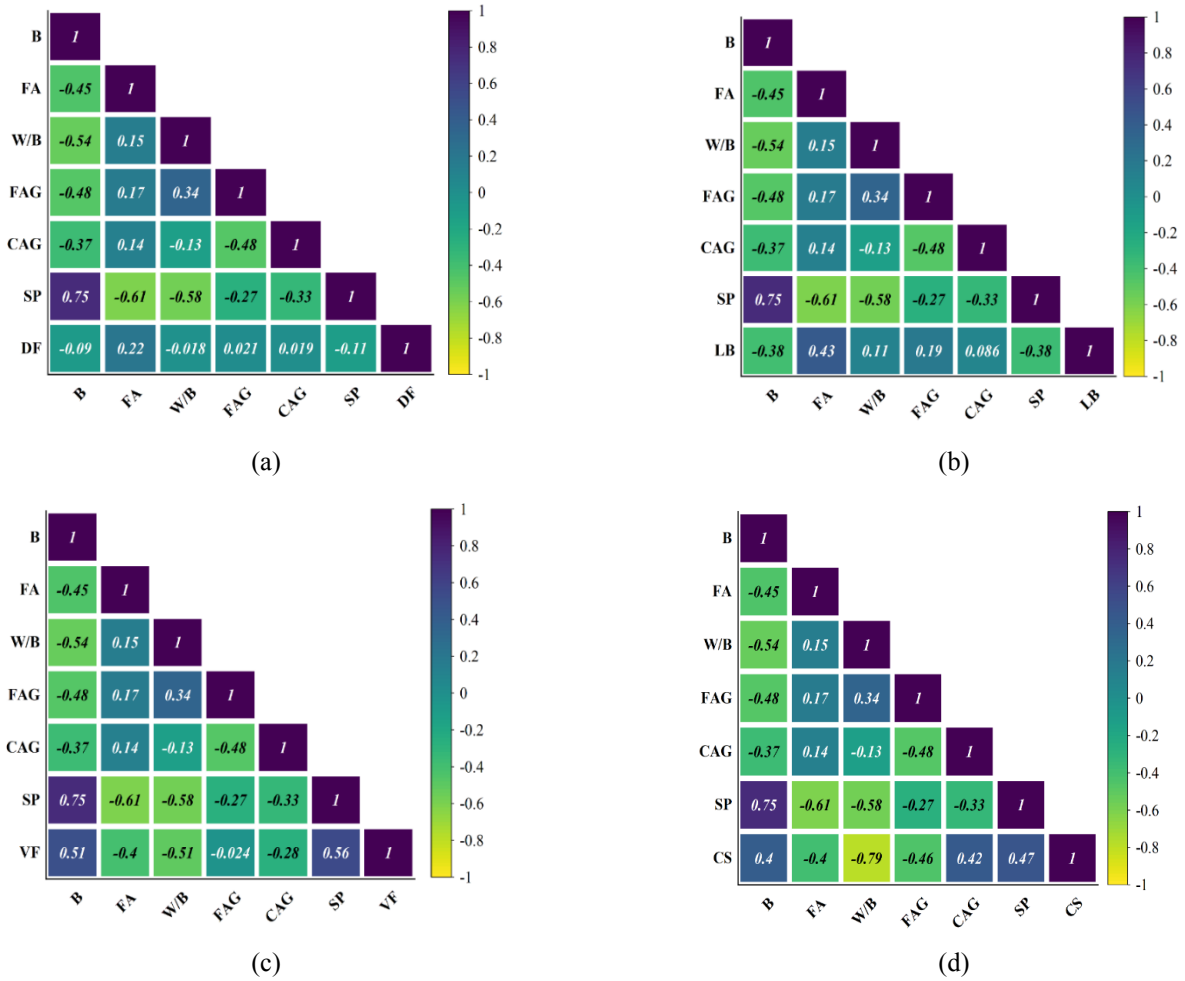

Fig. 2 The Pearson correlation coefficient matrix between inputs and outputs

2.2 Grey Wolf Optimization (GWO)

GWO presents a meta-heuristic method (Mirjalili et al., 2014). With strong social foundations, grey wolves live in groups. To achieve this goal, wolves have their responsibility, i.e., alpha wolves known as leaders, beta are superior, and omega role as a scapegoat. Based on the wolves' rank, they have pursued encircling, attacking, and hunting prey. This treatment is mathematically formulated in Eqs. (1-2) (Mirjalili et al., 2014).

$$\vec{D} = \left|\vec{C}.\overrightarrow{X_P}(t) - \vec{X}(t)\right| \quad (1)$$

$$\vec{X}(t+1) = \overrightarrow{X_P}(t) - \vec{A}.\vec{D} \quad (2)$$

$\vec{X}$: the grey wolf situation
$\overrightarrow{X_P}(t)$: the prey location vector
t : and the present moment

$$\vec{A} = 2\vec{a}.\overrightarrow{r_1} - \vec{a} \quad (3)$$

$$\vec{C} = 2.\overrightarrow{r_2} \quad (4)$$

a : linearly reduced from 2 to 0
$\overrightarrow{r_1}$, $\overrightarrow{r_2}$: random vectors spread between 0 and 1 monotonously

By assuming that the wolves are sufficiently near to the prey, the hunting tendency of wolves is simulated according to Fig. 3. The other wolves use alpha, beta, and omega positions to determine the position of the hunt. Here, the wolves' average position is utilized to determine the position of the hunt:

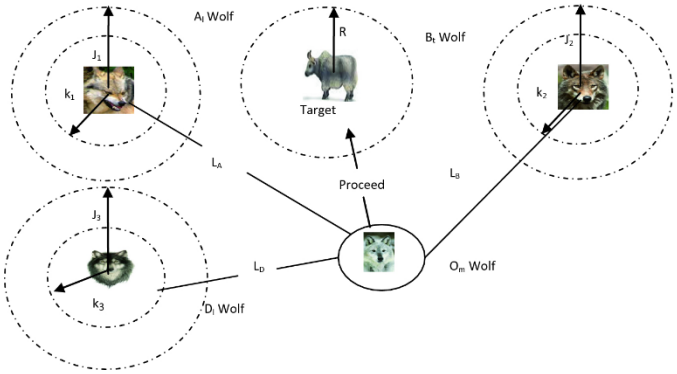

Fig. 3 How α, β, ω, and δ are defined in GWO (Mirjalili et al., 2014)

$$\left\{\begin{matrix}\overrightarrow{D_\alpha} = \left|\overrightarrow{C_1}.\overrightarrow{X_\alpha} - \vec{X}\right| \\ \overrightarrow{D_\beta} = \left|\overrightarrow{C_2}.\overrightarrow{X_\beta} - \vec{X}\right| \\ \overrightarrow{D_\delta} = \left|\overrightarrow{C_3}.\overrightarrow{X_\delta} - \vec{X}\right|\end{matrix}\right\}, \left\{\begin{matrix}\overrightarrow{X_1} = \overrightarrow{X_\alpha} - \overrightarrow{A_1}.\overrightarrow{D_\alpha} \\ \overrightarrow{X_2} = \overrightarrow{X_\beta} - \overrightarrow{A_2}.\overrightarrow{D_\beta} \\ \overrightarrow{X_3} = \overrightarrow{X_\delta} - \overrightarrow{A_3}.\overrightarrow{D_\delta}\end{matrix}\right\}, \vec{X}(t+1) = \frac{\overrightarrow{X_1}+\overrightarrow{X_2}+\overrightarrow{X_3}}{3} \quad (5)$$

After defining the prey position, the subsequent stage is exploitation, which is obtained from the vector A ⃗ when the value of variable a reduces from 2 to 0, wolves' locations go toward the location of the hunt. In addition, C could alter the prey's position and the complexity of the hunting task. The grey wolf is forced to veer away from the prey and find a better one by the variable X value being greater than 1. Once all wolves have gone through this procedure, the ideal site will be identified.

2.3 Artificial Hummingbird Optimization (AHA)

AHA is designed to address single-objective optimization problems. AHA is categorized as a bio-based method and falls under the broader class of swarm algorithms (Zhao et al., 2022). The optimization method involves the emulation of three distinct foraging behaviors by AHA, including directed foraging, territorial foraging, and migratory foraging. In the context of foraging activities, the simulation incorporates three distinct flying skills: axial flight, diagonal flight, and omnidirectional flight. The fundamental constituents of AHA are concisely delineated as follows.

Visit table: The visit table has significant importance within the AHA framework as it serves to monitor and record the visitation levels of individual hummingbirds to various food sources. The visit table's greater worth indicates a longer duration during which the hummingbird does not visit the food source. This implies that the food source collects a greater amount of nectar for the hummingbird, hence increasing its priority for visitation.

Guided foraging: Within the context of avian foraging behavior, the enhanced physical condition of a hummingbird serves as an indicator of the increased pace at which the nectar of the identified food source is replenished. During the guided foraging phase, it can be seen that each individual hummingbird has a tendency to choose the food source with the greatest visit level among the available options that possess the biggest nectar volume.

$$v_i(t+1) = x_{i,tar}(t) + D.a.\left(x_i(t) - x_{i,tar}(t)\right) \quad (6)$$

Let $x_i(t)$ represent the positional coordinates of the ith food source at time t. Similarly, $x_{i,tar}(t)$ denotes the positional coordinates of the target source where the ith hummingbird plans to visit. The guided factor, a, is a random variable that follows a typical normal distribution with mean 0 and standard deviation 1, displayed as N (0, 1).

Territorial foraging: During the territorial foraging phase, hummingbirds exhibit a preference for exploring their immediate vicinity rather than venturing to established food sources beyond their nearby zone.

$$v_i(t+1) = x_i(t) + D.b.x_i(t) \quad (7)$$

The variable b represents a territorial component that follows a conventional normal dispersion N (0,1).

Migration foraging: In instances when the availability of sustenance becomes limited within a particular habitat, hummingbirds have been shown to engage in migratory behavior, relocating to alternative regions to get nourishment. In the context of foraging behavior, a migration coefficient is established to regulate the timing of migratory activities.

$$x_{wor}(t+1) = Low + r.(Up - Low) \quad (8)$$

The source exhibiting the lowest nectar-refilling rate in the population is displayed as x_{wor}. The hummingbirds possess three distinct flying talents.

Axial flight: The ability of a hummingbird to navigate across the search space along any coordinate axis is referred to as axial flying.

$$D^{(i)} = \begin{cases}1 & if \quad i = randi([1,d]) \\ 0 & else\end{cases} \qquad i = 1, \dots, d \quad (9)$$

Diagonal flight: The concept of diagonal flying signifies the capability of a hummingbird to go from one corner of a rectangular area to the diagonally opposite corner during its quest for resources.

$$D^{(i)} = \begin{cases}1 & if \quad i = P(j), j\epsilon[1,k], P = randperm(k), k\epsilon\left[2, [r_1.(d-2)+1]\right] \\ 0 & else\end{cases} \quad i = 1, \dots, d \quad (10)$$

Omnidirectional flight: This part displays the capability of a hummingbird to navigate in a manner that encompasses all possible directions projected onto each of the coordinate axes inside the looking area.

$$D^{(i)} = 1, \qquad i = 1, \dots, d \quad (11)$$

Answer readjusts: When the candidate answer generated during the guided foraging or territorial foraging steps exhibits high quality compared to the present solution, the hummingbird will relinquish the present source and stay at the candidate resolution for the purpose of eating.

$$x_i(t+1) = \begin{cases}x_i(t) & f(x_i(t)) \le f(v_i(t+1)) \\ v_i(t+1) & f(x_i(t)) > f(v_i(t+1))\end{cases} \quad (12)$$

The function $f(\cdot)$ represents the fitness value, whereas $v_i(t+1)$ denotes the candidate solution at time $(t+1)$.

2.4 Hybrid Random Forests (RF) Schemes

The nonparametric approach Random Forest (RF) is often used in supervised machine learning (Breiman, 2001). The RF algorithm was developed by Breiman, whereby he introduced the concept of combining random parameter selection at each node with Bootstrap aggregation (Bagging). Based on the notion of the Decision Tree (DT), RF may be seen as an improved method of bagging. The underlying concept of RF is the use of bootstrap resampling to get multiple samples from the primary database, followed by the creation of a DT for each bootstrap sample. The DTs are mutually independent, and each DT is created by a random process in a RF. Consequently, an RF scheme has many separate predictors that have been independently built. The individual predictions for each tree are aggregated by means of averaging to get the final forecast (Han et al., 2020). The predicted result of the RF model $\hat{\tau}(x)$ might be calculated from an input characteristic vector $x = [x_1, x_2, \dots, x_n]^T$ using the formula in Eq. (13).

$$\hat{\tau}(x) = \frac{1}{B}\sum_{b=1}^{B}\hat{\tau}_b(x) \quad (13)$$

B stands for the entire quantity of trees, and $\hat{\tau}_b(x)$ stands for the approximate provided by the b_{th}tree. Due to its capacity to effectively eliminate extraneous input data by considering their relative significance, RF schemes have emerged as highly efficient supervised machine learning methodologies currently used.

2.5 Indices

Various efficiency assessors were used to gauge how well generated hybrid schemes performed in anticipating the features under consideration. To do this, the following accuracy measurements - R^2, RMSE, and MAE - were computed:

$$R^2 = \left(\frac{\sum_{p=1}^{P}(t_P - \bar{t})(y_P - \bar{y})}{\sqrt{[\sum_{p=1}^{P}(t_P - \bar{t})^2][\sum_{p=1}^{P}(y_P - \bar{y})^2]}}\right)^2 \quad (14)$$

$$RMSE = \sqrt{\frac{1}{P}\sum_{p=1}^{P}\left(y_p - t_p\right)^2} \quad (15)$$

$$MAE = \frac{1}{p}\sum_{p=1}^{p}|y_p - t_p| \quad (16)$$

where, y_p, t_p, $\bar{t}$, and $\bar{y}$ show the projected of the P^{th}, the goal of the P^{th}, the mean of the goal and, the mean of the projected.

3. Results and Discussion

The following information is provided as the outcome of the RF schemes used to anticipate SCC characteristics. As previously noted, choosing the optimal mixture of the hyperparameters is what determines the key variables in RF performance. Fig. 4 shows strong promises for approximation in the testing stage and also learning. For GWO-RF and AHA-RF, which are connected to the fresh and hardened characteristics of SCC, a comparison of the outcomes with those anticipated by created schemes is shown in Fig. 4. The suggested R^2 values throughout the learning and testing phases are adequate. It denotes good precision in the training and approximation processes since the connection among the measured and anticipated SCC qualities from hybrid schemes is satisfactory.

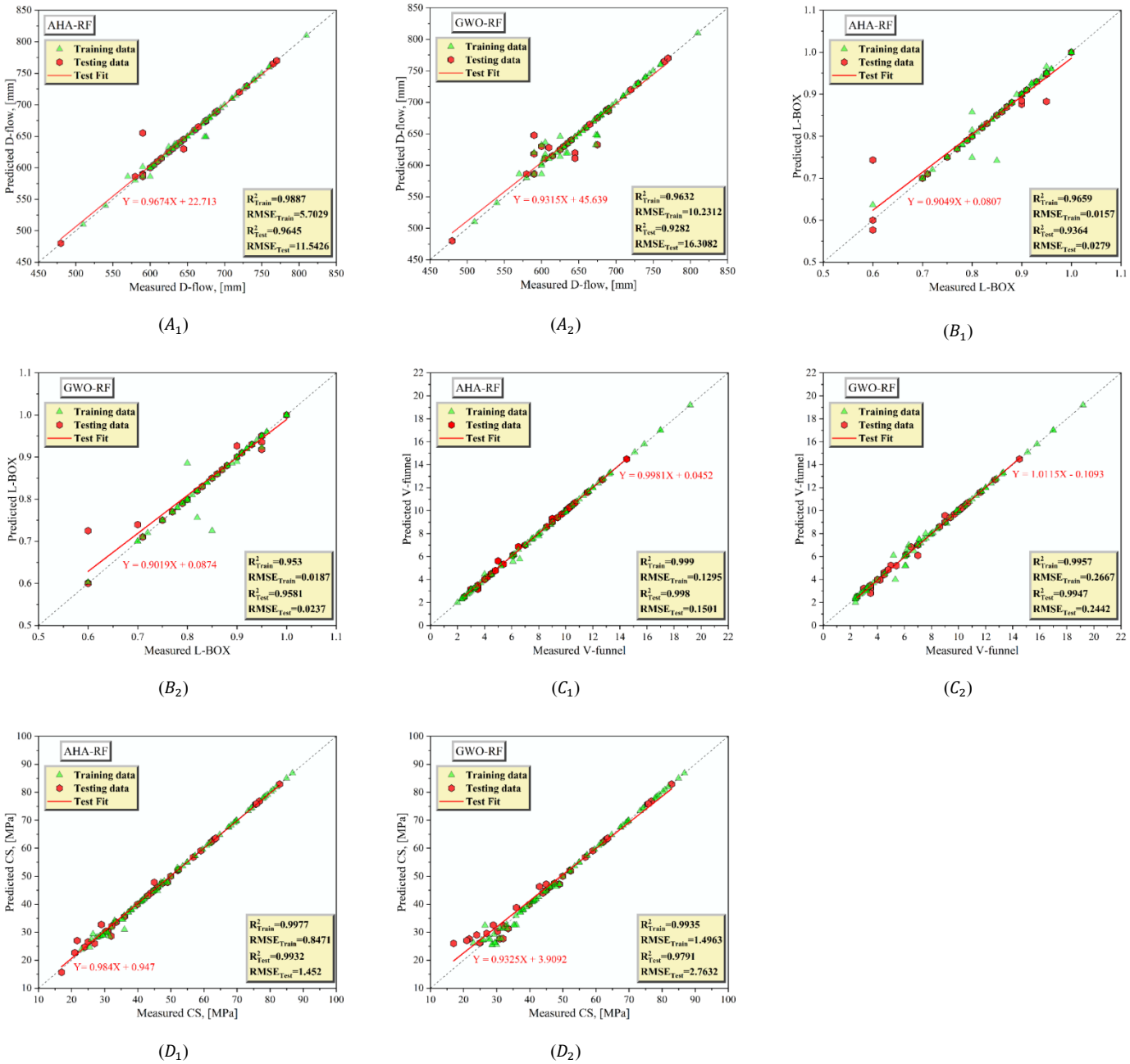

Fig. 4 Scatter plot

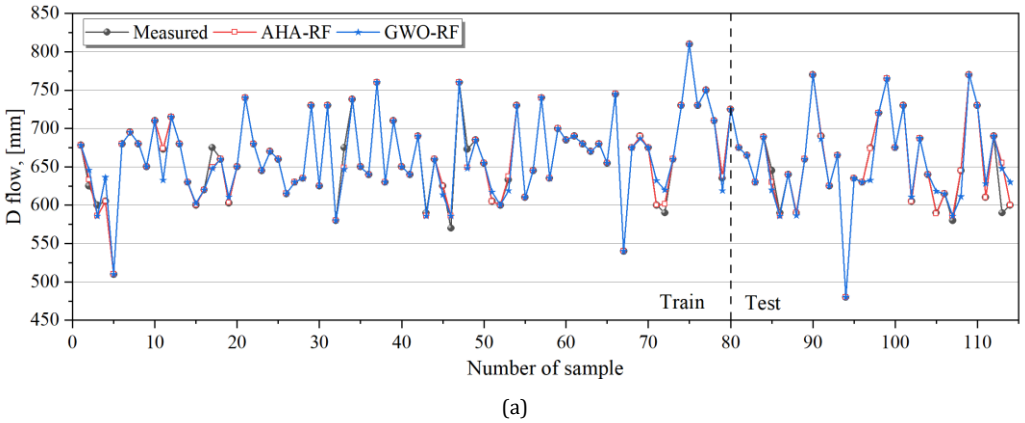

(a)

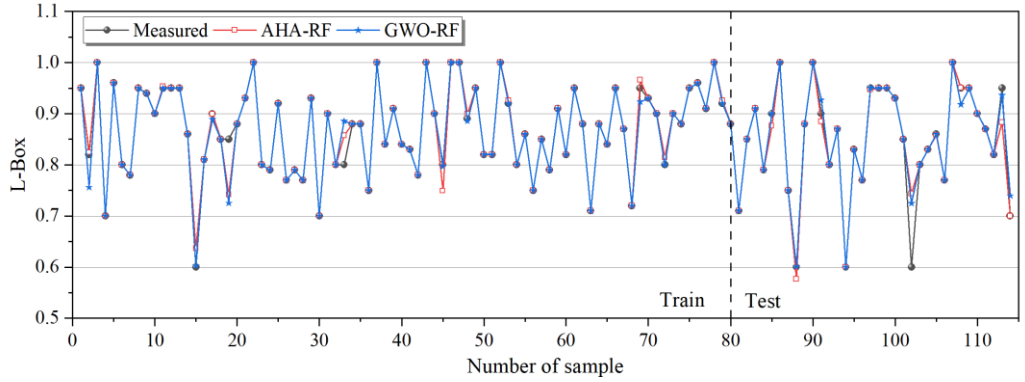

(b)

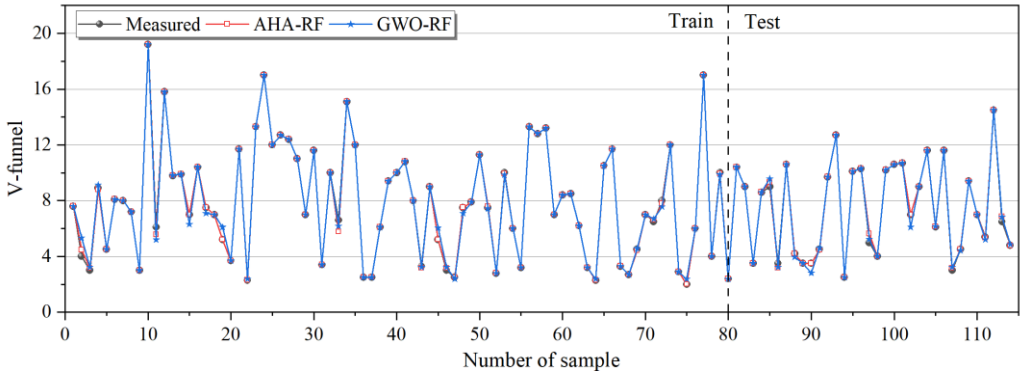

(c)

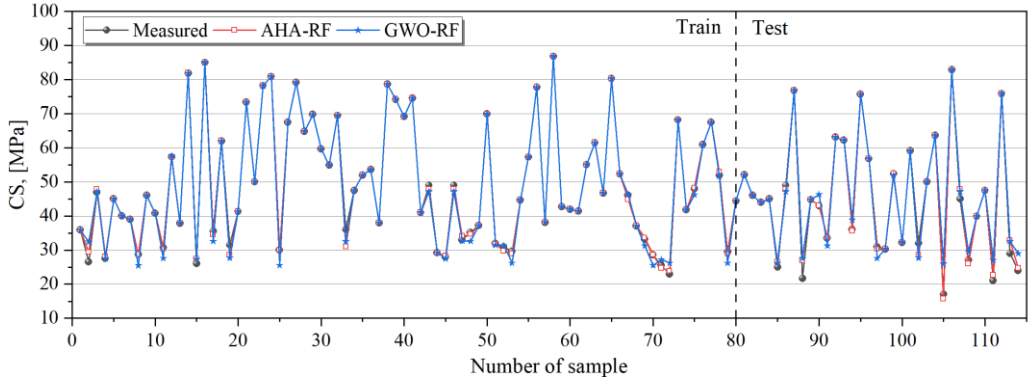

(d)

Fig. 5 Predictions by networks

Table 2. Metrics value of created RF networks

Properties	Metrics	Phase	$AHA-RF$	$GWO-RF$	(Saha et al., 2020)	(Kaveh et al., 2018)
$D\ flow$	R^2	Train	0.9887	0.9632	0.931	0.57
		Test	0.9645	0.9282		
	$RMSE$	Train	5.7029	10.2312	11.678	36.29
		Test	11.5426	16.3082		
	MAE	Train	1.7263	4.1898		27.66
		Test	2.7386	7.6096		
$L-box$	R^2	Train	0.9659	0.953	0.91	0.56
		Test	0.9364	0.9581		
	$RMSE$	Train	0.0157	0.0187	0.025	0.06
		Test	0.0279	0.0237		
	MAE	Train	0.0039	0.0040		0.05
		Test	0.0082	0.0070		
$V-funnel$	R^2	Train	0.999	0.9957	0.958	0.87
		Test	0.998	0.9947		
	$RMSE$	Train	0.1295	0.2667	0.723	1.46
		Test	0.1501	0.2442		
	MAE	Train	0.0378	0.1047		1.11
		Test	0.0579	0.1164		
CS	R^2	Train	0.9977	0.9935	0.955	0.93
		Test	0.9932	0.9791		
	$RMSE$	Train	0.8471	1.4963	3.783	4.45
		Test	1.452	2.7632		
	MAE	Train	0.3357	0.6987		3.45
		Test	0.7023	1.5834		

Additionally, Table 2 provides the outcomes of constructed schemes that took into account R^2, RMSE, and MAE values for the fresh and hardened characteristics of SCC. The outcomes of the schemes that have been put out in this investigation have been contrasted with the available research (Saha et al., 2020). The AHA-RF values for D flow are superior to both the research and GWO-RF. In training, for example, the RMSE value of the network by AHA is 5.7029mm, but this value for the GWO-RF model is approximately twice as high. Saha et al. (2020) are next with 11.67mm, followed by Kaveh et al. (2018) with 36.29mm. Outcomes from AHA-RF are superior to those from GWO-RF and the research in terms of L-box. For example, the RMSE of the AHA network in training is 0.0157, whereas this number for the GWO-RF scheme is 0.0187. Saha et al. (2020) comes in second place with a 0.025 RMSE value, followed by Kaveh et al. (2018) with a 0.06 RMSE value. When it comes to V-funnel outcomes, AHA-RF outperforms both research and GWO-RF by a wide margin. For example, the R2 value of the AHA model in the testing stage is 0.998, while for the GWO-RF is 0.9947. Saha et al. (2020) are next with a value of 0.958, followed by Kaveh et al. (2018) with a value of 0.87. The CS result, in addition, shows identical outcomes to those previously mentioned. Overall, the AHA-developed RF model performs better than others, demonstrating the AHA tactic's capacity to select the most advantageous variables for the approach under consideration.

The time series data shown in Figs. 5(a-d) may be used to determine a justified fit among observed values and forecasted values. As can be observed, for both of the suggested optimized RF (GWO-RF and AHA-RF) schemes' fresh and hardened characteristics of SCC, the calculated values show satisfactory agreement with measured ones, conveying the viability of the suggested integrated methods to predict the D flow, L box, V funnel, and CS with great accuracy. Time series data show that established schemes provide the minimum variance in the procedure of forecasting attributes, producing fairly correct anticipations that may be deployed in real-world settings.

4. Conclusions

Limited research has focused on predicting both the fresh (e.g., D-flow, L-box, V-funnel) and hardened (e.g., compressive strength, CS) characteristics of self-compacting concrete (SCC). Hence, the research endeavors to establish networks to anticipate SCC characteristics by the random forests (RF) method. In this work, we used artificial hummingbird algorithms (AHA) and GWO tactics to find the critical variables of the RF technique, which may be improved utilizing optimization methods. The following are the primary findings:

1) Outcomes show strong promise for learning and also approximate performance throughout testing. The suggested schemes' appropriate R^2 values throughout the learning and testing phases may be the outcome. It denotes good precision in the training and approximation processes since the connection among the measured and anticipated SCC qualities from hybrid schemes are satisfactory.
2) Based on D flow, the outcomes of AHA-RF are finer than GWO-RF and research. For example, the RMSE of the network by AHA in the training stage is 5.7029 mm, while for the GWO-RF is roughly twice.
3) Based on L-box, the findings of AHA-RF are finer than GWO-RF and research. For instance, the RMSE of the network by AHA in the raining stage is 0.0157, while for GWO-RF is 0.0187, followed by Saha et al. (2020) at 0.025, and then Kaveh et al. (2018) by 0.06.
4) In the V-funnel outcomes, the outcomes of AHA-RF are extremely better than GWO-RF and research. For example, R^2 of network by AHA in the testing stage is 0.998, while GWO-RF is 0.9947, followed by Saha et al. (2020) at 0.958, and then Kaveh et al. (2018) by 0.87.
5) The outcomes for CS show identical findings as before. In general, the AHA-developed RF model operates better than others, demonstrating the AHA tactic's capacity to select the best variables for the under-consideration technique.
6) The calculated values represent the viability of the recommended methods to anticipate the $D\ flow, L\ box, V\ funnel, and\ CS$ with great accuracy, showing an acceptable agreement with observed ones. Time series data displays that established schemes offer the minimum variance in the procedure of forecasting attributes, producing moderately precise anticipations that may be deployed in practical settings.
7) Despite the promising performance of the AHA-RF model in predicting both fresh and hardened properties of SCC, some limitations must be acknowledged. The dataset used may not fully represent all possible mix designs or environmental conditions encountered in real-world applications. Additionally, the study primarily focused on specific tests (slump flow, L-box, V-funnel, and compressive strength), potentially overlooking other relevant SCC characteristics such as durability, shrinkage, or rheology. Finally, while AHA and GWO were effective optimizers, the exploration of other methods of techniques could yield different or improved outcomes.
8) The proposed hybrid AHA-RF model can be a valuable tool for engineers and concrete technologists aiming to optimize SCC mix designs efficiently without relying solely on extensive experimental work. By accurately forecasting SCC performance metrics, the model aids in reducing material waste, saving time, and ensuring the desired performance for various structural and infrastructure applications. This approach is particularly beneficial in ready-mix concrete plants, precast industries, and quality control laboratories seeking to streamline production while maintaining high standards.
9) Future studies could expand the model by incorporating a broader range of input variables, including chemical admixtures, curing conditions, and environmental factors. Cross-validation with larger, more diverse datasets from different geographic regions would also enhance the model's generalizability. Moreover, integrating other advanced machine learning techniques or hybridizing AHA-RF with deep learning models may lead to further performance improvements in predicting SCC properties across a wider spectrum of applications.

Declarations

Availability of data and materials: Data is available upon request.

Authors' Contributions: The author contributed to the investigation's conception and configuration. Data collection, simulation and analysis were conducted by " Junsong Wang ".

References

Acharya, P. K., & Patro, S. K. (2015). Effect of lime and ferrochrome ash (FA) as partial replacement of cement on strength, ultrasonic pulse velocity and permeability of concrete. Construction and Building Materials, 94, 448–457. https://doi.org/10.1016/j.conbuildmat.2015.07.081

Aggarwal, Y., & Aggarwal, P. (2011). Prediction of compressive strength of SCC containing bottom ash using artificial neural networks. International Journal of Mathematical and Computational Sciences, 5(5), 762–767.

Aljarah, I., Faris, H., Mirjalili, S., & Al-Madi, N. (2018). Training radial basis function networks using biogeography-based optimizer. Neural Computing and Applications, 29(7), 529–553. https://doi.org/10.1007/s00521-016-2559-2

Bardhan, A., & Asteris, P. G. (2023). Application of hybrid ANN paradigms built with nature inspired meta-heuristics for modelling soil compaction parameters. Transp Geotech 41: 100995. https://doi.org/10.1016/j.trgeo.2023.100995

Beycioğlu, A., & Aruntaş, H. Y. (2014). Workability and mechanical properties of self-compacting concretes containing LLFA, GBFS and MC. Construction and Building Materials, 73, 626–635. https://doi.org/10.1016/j.conbuildmat.2014.09.071

Bi, Y., & Yi, Y. (2024). Application of a comparative analysis of random forest programming to predict the strength of environmentally friendly geopolymer concrete. Steel and Composite Structures, 50(4), 443–458. https://doi.org/10.12989/scs.2024.50.4.443

Bingöl, A. F., & Tohumcu, İ. (2013). Effects of different curing regimes on the compressive strength properties of self-compacting concrete incorporating fly ash and silica fume. Materials & Design, 51, 12–18. https://doi.org/10.1016/j.matdes.2013.03.106

Breiman, L. (2001). Random forests. Machine Learning, 45(1), 5–32. https://doi.org/10.1023/A:1010933404324

Debnath, P., & Dey, A. K. (2018). Prediction of bearing capacity of geogrid-reinforced stone columns using support vector regression. International Journal of Geomechanics, 18(2), 4017147. https://doi.org/10.1061/(ASCE)GM.1943-5622.0001067

Dehghanbanadaki, A., Khari, M., Amiri, S. T., & Armaghani, D. J. (2021). Estimation of ultimate bearing capacity of driven piles in c-φ soil using MLP-GWO and ANFIS-GWO models: a comparative study. Soft Computing, 25, 4103–4119. https://doi.org/10.1007/s00500-020-05435-0

Dhiyaneshwaran, S., Ramanathan, P., Baskar, I., & Venkatasubramani, R. (2013). Study on durability characteristics of self-compacting concrete with fly ash. Jordan Journal of Civil Engineering, 7(3), 342–352.

Douma, O. B., Boukhatem, B., Ghrici, M., & Tagnit-Hamou, A. (2017). Prediction of properties of self-compacting concrete containing fly ash using artificial neural network. Neural Computing and Applications, 28(1), 707–718. https://doi.org/10.1007/s00521-016-2368-7

Esmaeili Falak, M., Sarkhani Benemaran, R., & Seifi, R. (2020). Improvement of the Mechanical and Durability Parameters of Construction Concrete of the Qotursuyi Spa. Concrete Research, 13(2), 119–134. https://doi.org/10.22124/JCR.2020.14518.1395

falak, M. E., & Benmaran, R. S. (2024). Ensemble Extreme Gradient Boosting based models to predict the bearing capacity of micropile group.

Applied Ocean Research, 151. https://doi.org/10.1016/j.apor.2024.104149

Farrar, D. E., & Glauber, R. R. (1967). Multicollinearity in regression analysis: the problem revisited. The Review of Economic and Statistics, 92–107. https://doi.org/10.2307/1937887

Garcia-Troncoso, N., Li, L., Cheng, Q., Mo, K. H., & Ling, T.-C. (2021). Comparative study on the properties and high temperature resistance of self-compacting concrete with various types of recycled aggregates. Case Studies in Construction Materials, 15, e00678. https://doi.org/10.1016/j.cscm.2021.e00678

Gettu, R., Izquierdo, J., Gomes, P. C. C., & Josa, A. (2002). Development of high-strength self-compacting concrete with fly ash: a four-step experimental methodology. Proc. 27th Conf. on Our World in Concrete & Structures, CI-Premier Pte. Ltd., Eds. CT Tam, DWS Ho, P. Paramasivam y TH Tan, Singapore, 217–224.

Golafshani, E. M., & Pazouki, G. (2018). Predicting the compressive strength of self-compacting concrete containing fly ash using a hybrid artificial intelligence method. Computers and Concrete, 22(4), 419–437.

Guangyao, D., Songmin, L., Xiaoling, W., Yazhi, Z., & Qihang, W. (2024). Optimal design of ecological concrete mix proportions based on AHP-GWO-BP neural network. International Journal of Environmental Research, 18(2), 24. https://doi.org/10.1007/s41742-023-00562-6

Güneyisi, E., Gesoğlu, M., & Özbay, E. (2010). Strength and drying shrinkage properties of self-compacting concrete incorporating multi-system blended mineral admixtures. Construction and Building Materials, 24(10), 1878–1887. https://doi.org/10.1016/j.conbuildmat.2010.04.015

Han, H., Jahed Armaghani, D., Tarinejad, R., Zhou, J., & Tahir, M. M. (2020). Random forest and bayesian network techniques for probabilistic prediction of flyrock induced by blasting in quarry sites. Natural Resources Research, 29(2), 655–667. https://doi.org/10.1007/s11053-019-09611-4

Jalal, M., Pouladkhan, A., Harandi, O. F., & Jafari, D. (2015). Comparative study on effects of Class F fly ash, nano silica and silica fume on properties of high performance self-compacting concrete. Construction and Building Materials, 94, 90–104.

Kalemci, E. N., İkizler, S. B., Dede, T., & Angın, Z. (2020). Design of reinforced concrete cantilever retaining wall using grey wolf optimization algorithm. Structures, 23, 245–253. https://doi.org/10.1016/j.istruc.2019.09.013

Kaveh, A., Bakhshpoori, T., & Hamze-Ziabari, S. M. (2018). M5'and Mars based prediction models for properties of self-compacting concrete containing fly ash. Periodica Polytechnica Civil Engineering, 62(2), 281–294. https://doi.org/10.3311/PPci.10799

Kostić, S., & Vasović, D. (2015). Prediction model for compressive strength of basic concrete mixture using artificial neural networks. Neural Computing and Applications, 26(5), 1005–1024.

Krishnapal, P., Yadav, R. K., & Rajeev, C. (2013). Strength characteristics of self-compacting concrete containing fly ash. Res J Eng Sci ISSN, 2278, 9472. https://doi.org/10.1007/s00521-014-1763-1

Liu, D. (2025). Application of tuned random forests model on cement paste including fly ash and MgO expansive additive. Multiscale and Multidisciplinary Modeling, Experiments and Design, 8(1), 1–18. https://doi.org/10.1007/s41939-024-00651-9

Liu, J., Yan, K., Zhao, X., & Hu, Y. (2016). Prediction of autogenous shrinkage of concrete by support vector machine. International Journal of Pavement Research and Technology, 9(3), 169–177. https://doi.org/10.1016/j.ijprt.2016.06.003

Mahalingam, B., & Nagamani, K. (2011). Effect of processed fly ash on fresh and hardened properties of self-compacting concrete. Int J Earth Sci Eng, 4(5), 930–940.

Mirjalili, S., Mirjalili, S. M., & Lewis, A. (2014). Grey wolf optimizer. Advances in Engineering Software, 69, 46–61. https://doi.org/10.1016/j.advengsoft.2013.12.007

Muthupriya, P., Sri, P. N., Ramanathan, M. P., & Venkatasubramani, R. (2012). Strength and workability character of self-compacting concrete with GGBFS, FA and SF. Int J Emerg Trends Eng Dev, 2(2), 424–434.

Naseri, F., Jafari, F., Mohseni, E., Tang, W., Feizbakhsh, A., & Khatibinia, M. (2017). Experimental observations and SVM-based prediction of properties of polypropylene fibres reinforced self-compacting composites incorporating nano-CuO. Construction and Building Materials, 143, 589–598. https://doi.org/10.1016/j.conbuildmat.2017.03.124

Nepomuceno, M. C. S., Pereira-de-Oliveira, L. A., & Lopes, S. M. R. (2014). Methodology for the mix design of self-compacting concrete using different mineral additions in binary blends of powders. Construction and Building Materials, 64, 82–94. https://doi.org/10.1016/j.conbuildmat.2014.04.021

Özcan, F., Atiş, C. D., Karahan, O., Uncuoğlu, E., & Tanyildizi, H. (2009). Comparison of artificial neural network and fuzzy logic models for prediction of long-term compressive strength of silica fume concrete. Advances in Engineering Software, 40(9), 856–863. https://doi.org/10.1016/j.advengsoft.2009.01.005

Patel, R. (2004). Development of statistical models to simulate and optimize self-consolidating concrete mixes incorporating high volumes of fly ash.

Pazouki, G., Golafshani, E. M., & Behnood, A. (2021). Predicting the compressive strength of self-compacting concrete containing Class F fly ash using metaheuristic radial basis function neural network. Structural Concrete. https://doi.org/10.1002/suco.202000047

Rashedi, K. A., Ismail, M. T., Hamadneh, N. N., Wadi, S., Jaber, J. J., & Tahir, M. (2021). Application of Radial Basis Function Neural Network Coupling Particle Swarm Optimization Algorithm to Classification of Saudi Arabia Stock Returns. Journal of Mathematics, 2021. https://doi.org/10.1155/2021/5593705

Saha, P., Debnath, P., & Thomas, P. (2020). Prediction of fresh and hardened properties of self-compacting concrete using support vector regression approach. Neural Computing and Applications, 32(12), 7995–8010. https://doi.org/10.1007/s00521-019-04267-w

Saha, P., Sapkota, S. C., Das, S., & Kwatra, N. (2024). Prediction of fresh and hardened properties of self-compacting concrete using ensemble soft learning techniques. Multiscale and Multidisciplinary Modeling, Experiments and Design, 7(5), 4923–4945. https://doi.org/10.1007/s41939-024-00423-5

Şahmaran, M., Yaman, İ. Ö., & Tokyay, M. (2009). Transport and mechanical properties of self-consolidating concrete with high volume fly ash. Cement and Concrete Composites, 31(2), 99–106. https://doi.org/10.1016/j.cemconcomp.2008.12.003

Sfikas, I. P., Badogiannis, E. G., & Trezos, K. G. (2014). Rheology and mechanical characteristics of self-compacting concrete mixtures containing metakaolin. Construction and Building Materials, 64, 121–129. https://doi.org/10.1016/j.conbuildmat.2014.04.048

Shadi, R., & Nazari, A. (2019). RETRACTED ARTICLE: Predicting the effects of nanoparticles on early age compressive strength of ash-based geopolymers by artificial neural networks. Neural Computing & Applications, 31, 743–750.

Shariati, M., Mafipour, M. S., Ghahremani, B., Azarhomayun, F., Ahmadi, M., Trung, N. T., & Shariati, A. (2020). A novel hybrid extreme learning machine–grey wolf optimizer (ELM-GWO) model to predict compressive strength of concrete with partial replacements for cement. Engineering with Computers, 1–23. https://doi.org/10.1007/s00366-020-01081-0

Siddique, R., Aggarwal, P., & Aggarwal, Y. (2012). Influence of water/powder ratio on strength properties of self-compacting concrete containing coal fly ash and bottom ash. Construction and Building Materials, 29, 73–81. https://doi.org/10.1016/j.conbuildmat.2011.10.035

Sonebi, M., Cevik, A., Grünewald, S., & Walraven, J. (2016). Modelling the fresh properties of self-compacting concrete using support vector machine approach. Construction and Building Materials, 106, 55–64. https://doi.org/10.1016/j.conbuildmat.2015.12.035

Subaşı, S., Beycioğlu, A., Sancak, E., & Şahin, İ. (2013). Rule-based Mamdani type fuzzy logic model for the prediction of compressive strength of silica fume included concrete using non-destructive test results. Neural Computing and Applications, 22(6), 1133–1139. https://doi.org/10.1007/s00521-012-0879-4

Sukumar, B., Nagamani, K., & Raghavan, R. S. (2008). Evaluation of strength at early ages of self-compacting concrete with high volume fly ash. Construction and Building Materials, 22(7), 1394–1401. https://doi.org/10.1016/j.conbuildmat.2007.04.005

Taffese, W. Z., & Nunes, S. (n.d.). MACHINE LEARNING-BASED PREDICTION OF SCC MORTAR PROPERTIES ACROSS VARIOUS CEMENT TYPES.

Tunca, O. (2024). Effect of the soil slope on the cost-efficient optimum discrete design of reinforced concrete isolated footings. Structures, 59, 105769. https://doi.org/10.1016/j.istruc.2023.105769

Uysal, M., & Yilmaz, K. (2011). Effect of mineral admixtures on properties of self-compacting concrete. Cement and Concrete Composites, 33(7), 771–776. https://doi.org/10.1016/j.cemconcomp.2011.04.005

Wang, J., Dai, Q., & Si, R. (2022). Experimental and Numerical Investigation of Fracture Behaviors of Steel Fiber–Reinforced Rubber Self-Compacting Concrete. Journal of Materials in Civil Engineering, 34(1), 4021379. https://doi.org/10.1061/(ASCE)MT.1943-5533.0004010

Yang, H. Y., & Dong, Y. F. (2013). Modelling concrete strength using support vector machines. Applied Mechanics and Materials, 438, 170–173. https://doi.org/10.4028/www.scientific.net/AMM.438-439.170

Yang, S., Fang, C. Q., & Yuan, Z. J. (2014). Study on mechanical properties of corroded reinforced concrete using support vector machines. Applied Mechanics and Materials, 578, 1556–1561. https://doi.org/10.4028/www.scientific.net/AMM.578-579.1556

Yazdi, J. S., Kalantary, F., & Yazdi, H. S. (2013). Prediction of elastic modules of concrete using support vector committee method. Journal of Materials in Civil Engineering, 25(1), 9–20. https://doi.org/10.1061/(ASCE)MT.1943-5533.0000507

Yoo, S.-W., Ryu, G.-S., & Choo, J. F. (2015). Evaluation of the effects of high-volume fly ash on the flexural behavior of reinforced concrete beams.

Construction and Building Materials, 93, 1132–1144. https://doi.org/10.1016/j.conbuildmat.2015.05.021

Yunpeng, L., Shenghuan, D., Yingbin, J., & Yuqian, M. (2024). Estimation of pile-bearing capacity applying hybrid auto-regressed models based on regression decision tree. Multiscale and Multidisciplinary Modeling, Experiments and Design, 7(3), 2225–2239. https://doi.org/10.1007/s41939-023-00330-1

Zhao, W., Wang, L., & Mirjalili, S. (2022). Artificial hummingbird algorithm: A new bio-inspired optimizer with its engineering applications. Computer Methods in Applied Mechanics and Engineering, 388, 114194. https://doi.org/10.1016/j.cma.2021.114194

Disclaimer